X-VUV spectroscopic imaging with a micropattern gas detector

D. Pacella[a], R. Bellazzini[b,*], A. Brez[b], G. Pizzicaroli[a], M. Finkenthal[c,1]

[a] *Associazione EURATOM-ENEA sulla Fusione, CR Frascati, 00044 Frascati, Rome, Italy*
[b] *INFN-Sezione di Pisa, University of Pisa, Via Bounarroti 2, Pisa 56127, Italy*
[c] *Plasma Spectroscopic Group, Johns Hopkins University, Baltimore, MD 21218, USA*

Abstract

An innovative system which combines very fast 2D imaging capabilities with spectral resolution in the X-VUV range 0.2–8 keV has been developed at ENEA-Frascati (Italy) in collaboration with INFN-Pisa (Italy). It is based on a pinhole camera coupled to a micropattern gas detector having a gas electron multiplier as gas amplifying stage. This detector (2.5 cm × 2.5 cm active area), equipped with a 2D read-out printed circuit board with 144 pixels in a square matrix geometry (12 × 12) has been adapted to work at low energy, as far as 0.2 keV, in various configurations. Spectra with different X-VUV laboratory sources, energy calibrations curves and detection efficiency are discussed for all the proposed configurations. Thanks to the high photon flux (10^6 ph/s mm^2) detected by this device, high time resolution can be obtained (framing rates up to 100 kHz). The full system has been tested on the Frascati Tokamak Upgrade in 2001 and on the National Spherical Tokamak eXperiments (NSTX) in 2002 as a possible diagnostic tool for magnetic fusion plasmas. Time-resolved 2D images are presented. These results open the way to a new X-VUV imaging technique, where the low definition (limited number of pixels) is highly compensated by the strongly enhanced contrast due to the fine and controlled energy discrimination and by the capability to get images in a selected energy range. The innovative combination of these two major characteristics, make this device a candidate for applications beyond the magnetic plasma physics field.

1. Introduction

A new imaging device in the soft-X-ray range, developed in the framework of a collaboration between ENEA-Frascati (Italy) and INFN-Pisa (Italy), was recently introduced as diagnostic for magnetic fusion plasmas [1]. A prototype device was set up and tested in laboratory and then operated in a preliminary configuration with a few pixels, on the Frascati Tokamak Upgrade (FTU).

In this work, the spectroscopic capabilities of the instrument have been explored in the range 0.2–8 keV and based on this experience, an

---

*Corresponding author. Tel.: + 39-050-2214-367.

E-mail address: bellazzini@pi.infn.it (R. Bellazzini).

[1] Permanent address: Racah Institute, Hebrew University, Jerusalem, Israel.

X-VUV, 2D imaging device with energy discrimination and high time resolution, is now proposed. In the first part of the paper the spectroscopic capabilities as obtained on single pixels, will be discussed. Results on extended magnetic fusion plasmas, obtained at the National Spherical Tokamak eXperiment (NSTX), Princeton, (USA), are presented in the second part to show the capabilities of this new imaging instrument. The innovative combination of these two major

characteristics make it a candidate for applications beyond the magnetic plasma physics field.

2. Detector

2.1. MPGD with GEM

The micropattern gas detector (MPGD) [2] has a "conversion" region, delimited by the entrance
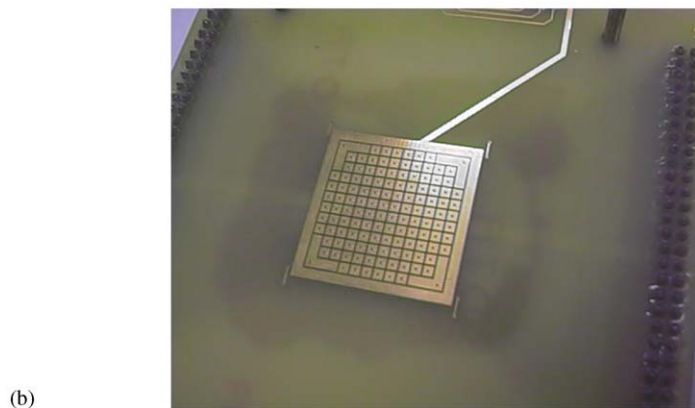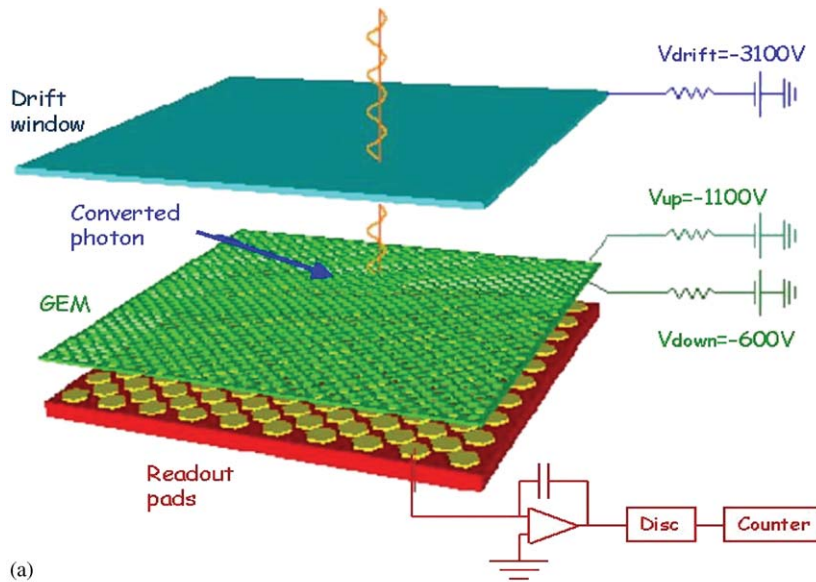
Fig. 1. (a) Schematic of the detection system, (b) PCB of the MPGD, with the read-out formed by squared pixels 2 mm × 2 mm (with the exception of the angular ones) drawn in a squared matrix 12 × 12.

window (cathode) and the upper face of the gas electron multiplier (GEM) foil, of 8 mm in order to have a good detection efficiency in a quite broad energy range (1–8 keV), relevant for magnetic fusion plasmas (Fig. 1a). The "transfer" region, between the lower face of the GEM and the read-out printed circuit board (PCB), is 1.3 mm. The GEM foil [3] is a thin kapton foil, metal-clad on both sides and pierced by a high density of narrow holes (typically 60 μm of diameter and 95 μm of pitch). The read-out board (Fig. 1b), with 144 pixels (12 × 12), has been designed to have high count rate, large gain range, good spatial resolution and a moderate number of pixels, each one connected to its independent acquisition channel. The size of the pixel is 2 mm × 2 mm and the full active area of the detector is 2.5 cm × 2.5 cm. The drift electric field is about 2.5 kV/cm while the transfer field is 4.5 kV/cm. The voltage difference applied to the faces of the GEM foil is in the range 450–500 V, depending on the required gain for the detector. In order to maximize the detector gain,

the count rates (of the order of 5×10^6 ph/s pixel) and the efficiency in the energy range of 0.2–8 keV, a mixture at atmospheric pressure of Ne (80%) and DME (20%) has been chosen.

2.2. MPGD for X-VUV domain

The standard window used in the past experiments, a Mylar foil with Al coating, has been replaced with an ultra-thin window (MOXTEK model ProLine 20) made by a polypropylene foil (0.3 μm), covered by a layer of a few thousands Angstroms of aluminum, sustained by an hexagonal metallic grid. Transparency of this window is plotted in Fig. 2 (black curve) and it permits to work at very low energy, up to 0.1 keV. Since below 3 keV air absorption is relevant, even for a few centimeters, it is necessary to remove the air between the X-ray source and the MPGD detector. In order to do that, the front of the detector was modified. The top part of the detector has been made of delrin, an insulating material hard
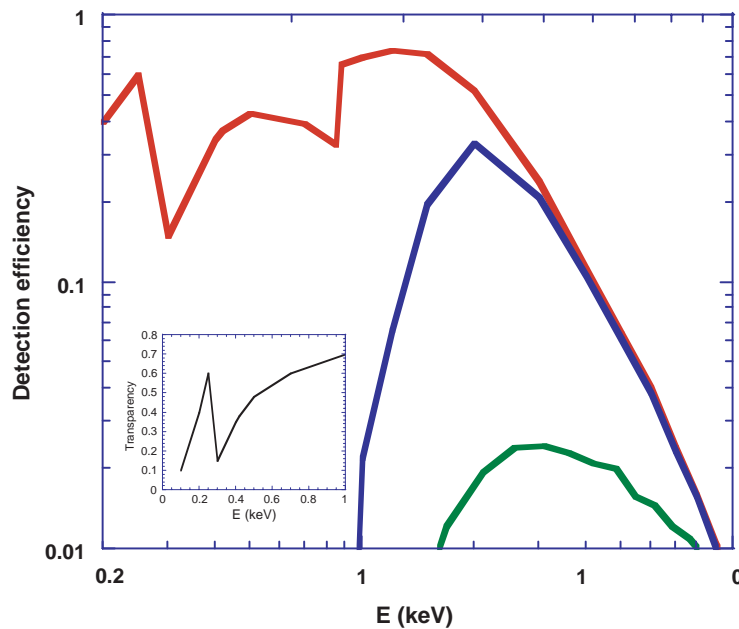
Fig. 2. Detection efficiency curves vs. photon energy for: detector connected to the source with vacuum in between (red curve), detector with a beryllium window of 12 μm and He in between (blue curve), detector with a beryllium window of 400 μm and air (10 cm) in between (green curve). In the bottom-left part of the figure is the plot of the transparency of the ultra-thin window mounted in the detector.

enough to be machined as a conflact fitting with rubber gasket. The ultra-thin window is mounted, by means of a rubber o-ring and a counter frame, to one side of the delrin interface, whose other side is connected, through conflact fittings, to the X-ray source under vacuum. Delrin allows a low vacuum, enough to avoid air absorption. The use of an insulator for this interface is requested since the window is supplied with 3000–3500 V; in low vacuum (or He), these voltage differences over many millimeters would otherwise cause discharges through the residual gas of the pumped volume. In our case, a 2 cm thick interface was enough to avoid this problem.

This large entrance window has a low gas transparency (10^{-3} Torr l/s) but cannot sustain an atmosphere of pressure gradient without additional sustaining structure. To work at a photon energy of 1 keV, it is enough to fill with He the volume between the source and the detector. In this case there are no pressure gradients on the ultra-thin window. This is the configuration that has been tested in the Tokamak experiments. To work in vacuum, a metallic grid has been glued on the ultra-thin window, with wires 100 μm thick and a pitch of 200 μm. This solution for vacuum has been used in laboratory with a VUV-X-ray source. In Fig. 2, the detection efficiency curves are plotted, for three configurations:

(1) ultra-thin window on the detector, window on the source of 400 μm of Be and 10 cm air between window and detector.
(2) ultra-thin window on the detector, window on the source of 12 μm of Be and 10 cm filled with He between the window and the detector.
(3) ultra-thin window on the detector and vacuum between source and detector.

3. Electronics

The electron charge corresponding to the detected X-ray photon, is collected at the pixel and processed by a fast charge pre-amplifier (LABEN 5231) and an amplifier (LABEN 5185). The resulting pulse has a Gaussian-like shape, with 50 ns of FWHM. The peak value is proportional to the total electronic charge collected on the pixel, with a conversion factor of about 1 μV/e^-. The noise (rms) is about 2000 e^-. With a threshold of 20 mV, the electronic noise is completely cut off for all channels. Discriminators and counters for a total of 128 channels form the data acquisition system, carried out in VME standard by CAEN. The threshold of the discriminator is programmable from 5 to 255 mV. The data acquisition system has been designed to use this X-ray imaging device in Tokamak experiments. Both in FTU and in NSTX, the plasma shot lasts about 1.5 s but most of the interesting processes to be studied occur on the time scale from 1 ms to 1 μs. Consequently, the software has been developed to allow the acquisition of many time frames (up to hundreds). The duration, the framing rate (from 1 kHz to 1 MHz) and all the values of the thresholds can be preset. The minimum dead time between two different time intervals of acquisition is 0.25 ms.

The fast, low-noise electronics coupled to the discriminators and asynchronous scalers ensure high-quality data affected by statistical noise only, with single photon counting at high rates (up to 5×10^6 ph/s pixel for a measured channel dead time of 170 ns), and high framing rates (up to 100 kHz).

4. Spectra in the X-VUV domain

4.1. X-VUV source

The X-ray laboratory source is a stable and reproducible source of K-shell emissions of light elements. Electrons emitted by a tungsten wire are accelerated, in a high-voltage gap (2–8 kV), normally against an anode made by various materials (Fe, Mg, O, C, B, Be) exciting the K-shell transitions. The emitted X-ray photons are observed at 45° to the normal. Apart from C (pure graphite anode), all the other elements are deposited on an Mg alloy substrate. Table 1 shows the elements, and the relative values used in these experiments.

Emissions are mainly in the K_α lines, with a small contribution at high energy (more than 1 keV) of continuum due to the bremsstrahlung

Table 1
Anode elements, emission lines, tube settings and emissivities of the X-VUV sources used in this work

Elements	K_{α} line (eV)	K_{α} line (Å)	Line width (Å)	HV (KV)	Current (mA)	Emissivity (10^{11} photons/s sr)
Mg	1250	9.89	0.05	8	0.16	1.3
O	523	23.6	0.25			
C	277	44.7	1.35	8	0.16	2.9
B	183	67.6	1.5	55	0.1	0.7
Be	112	114	6.4		0.1	0.37

emission of the decelerated electrons. A small contribution (a few percent) of Mg (anode substrate) and O is always present in the spectra; the O emissions can be observed only in vacuum configuration of MPGD because air absorbs entirely this wavelength. The emitted photons escape through a very thin window (1 mm × 10 mm) with a small divergence (about 1milliradian). Inside the source container, a Single Wire Proportional Counter (SWPC) is placed viewing the source at 45°. This SWPC is filled with a mixture P-50 (argon 50%–methane 50%) at pressures from 400 to 85 Torr and anode voltage from 1000 to 1500 V. The spectra thus obtained, have been used as check and validation of the spectra recorded with MPGD.

4.2. Experimental configurations

Several spectra have been acquired with the MPGD in different configurations, with ultra-thin window, single or double gem, with gas (He) or vacuum in front of the detector. The main goal of these studies was to demonstrate that each pixel of the detector behaves like an independent spectrometer, assessing energy resolution and efficiency in different energy ranges (configurations). The experimental results are organized in three groups, depending on the experimental configurations of the detector and the X-ray source:

(a) single GEM, He between source and detector, Mg source.
(b) double GEM, He between source and detector, C source.
(c) double GEM, vacuum between source and detector, B source
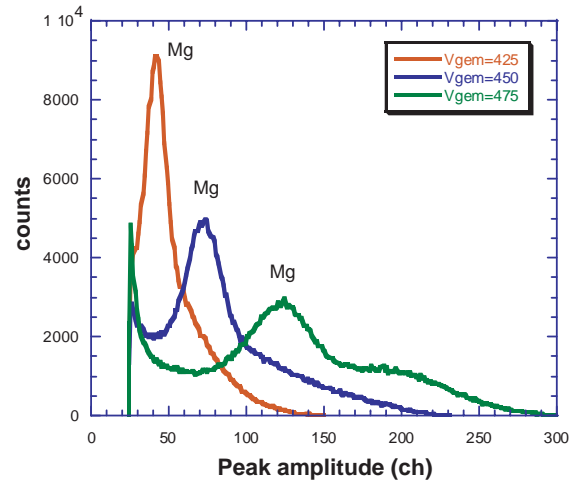
Fig. 3. Spectra of Mg (1250 eV) for three different values of the GEM voltage, with single GEM and He between source and detector.

Spectra were obtained on single pixel, connecting the output of the LABEN amplifier to a spectroscopic amplifier and then to a multi-channel analyzer (MCA). The electronic noise is always below the threshold of the MCA and therefore does not appear in the spectra.

(a) This configuration has been checked with the K_{α} line of Mg. In Fig. 3a, few spectra are presented, for different gains of the detector (GEM voltages from 425 to 475 V and Ne = 90%–DME = 10%,). The proportionality between the pulse amplitude and the detector gain has been checked as well as the constancy of counts with changing gain. Both these features are good indicators of a proper
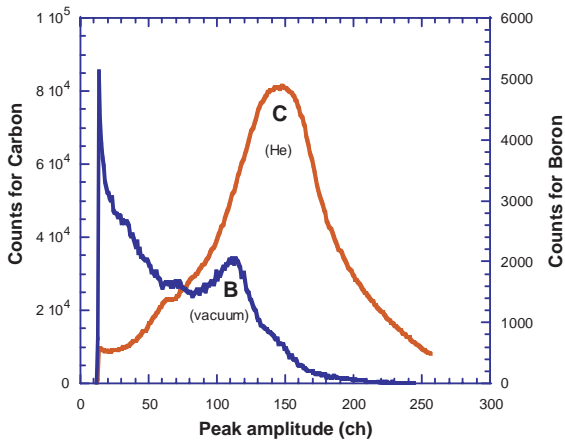
Fig. 4. Spectrum of carbon (277 eV, right axis) with double GEM and He between source and detector. Spectrum of boron (183 eV, left axis), with double GEM and vacuum between source and detector.

working of the detector. In this case, the energy resolution ΔE (FHWW)/E goes from 25% to 17% by increasing the gain.

(b) This configuration permits to work down to the energy of K_α of C (277 eV) with only moderate absorption due to a few centimeters of He. In Fig. 4 (red curve) the spectrum of C is shown, with a voltage of 390 V for each GEM foil and a total gain of about 3×10^4. The energy resolution (ΔE (FWHW)/E) is about 30%. The continuum component of the spectrum, for energy lower than the carbon line (277 eV), is absorbed by He, whose cut off, in this condition, is about 200–220 eV. In this case too, the proportionality with gain and the constancy of the counts have been checked.

(c) Ultra-thin window, double GEM, vacuum between source and detector.

At very low photon energy or for long source–detector distances, vacuum is required in between, instead of He. To study this configuration, the spectra of B have been obtained for different gains. In Fig. 4 (blue curve), the spectrum of B is shown, in the same conditions as those used for C. The line emission of boron (183 eV) is much less intense than that of carbon, since the source emissivity,

with a B anode, is approximately a factor 5 less than for C (see Table 1); also, the detector has a lower efficiency at 183 eV. The spectrum of B reveals the continuum emissions at low energy because in this configuration the detector is sensitive up to 0.1 keV. For photons of energy less than B (183 eV), the detector looses the energy resolution because of the large fluctuations of the number of the primary electrons produced by the photoelectron.

5. Energy calibration

Since NTU [4,5] and NSTX [6,7] Tokamak plasmas are tremendously intense X-VUV sources, the easier and more versatile configuration "a" (single GEM with He and ultra-thin window), assures, in the broad energy range 1–8 keV, enough counts even at the highest time resolution. In the previous section, we demonstrated the capability of the detector to measure spectra, even at very low energy, on a single pixel, and we estimated also the energy resolution in this case. This information is used to assess the spectral response of the detector in presence of continuum emissions. The detector is polarized with an electric field of the transfer gap of 5 kV/cm and electric field of the drift gap of 2.4 kV/cm.

The spectrum of Mg is shown in Fig. 5 for different values of the HV of the tube and with $V_{GEM} = 450$ V and Ne = 90% − DME = 10%. The spectrum is formed by a peak corresponding to the K_α line emission, whose broadening ($\Delta E/E \sim 20\%$) is entirely due to the energy resolution of the detector (the intrinsic line width is 0.5%) plus a continuum due to the bremsstrahlung emissions of the electrons on the Mg anode. The spectra are normalized to the Mg peak. The tail of the spectrum depends on the maximum energy of the accelerated electrons (H.V from 2 to 7 kV), on the energy resolution of the detector and on its efficiency. The spectra exhibit clearly the energy resolution property, in a broad range. For a quantitative analysis, we can consider that the measured spectrum $M(E)$ is a convolution between the spectral distribution of the source $S(E)$, weighted by the detection efficiency $D(E)$, and the

dominant instrumental broadening $R(E - E')$:

$$M(E) = \int_{E_{min}}^{E_{max}} S(E')D(E')R(E - E') \, dE',$$
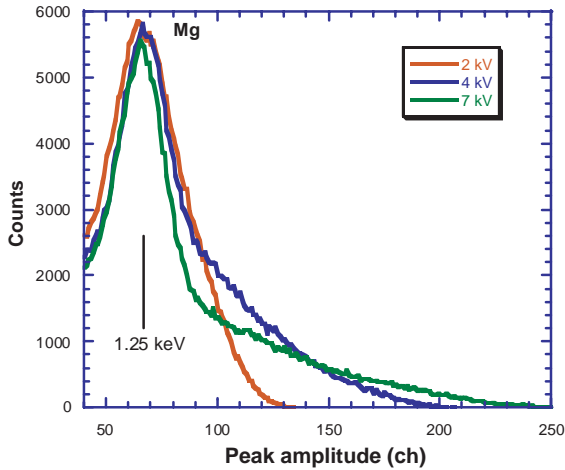
Fig. 5. Spectra of Mg (1.25 keV) with different Voltages for the anode of the X-ray source: 2.5 kV (red), 4 kV (blue), 7 kV (green). Spectra are normalized to the peak emission of the K feature.

where $R(E - E')$ has been estimated, for different energies, by means of the K spectra obtained with various elements (previous paragraph). Many pure continuum spectra have been produced using a portable, bright and compact X-ray tube, having a silver anode, powered by an adjustable high voltage up to 35 kV. With HV lower than 20 kV, we obtain almost pure continuum spectra (the K lines of silver are excited at energy higher than 20 keV). Many spectra have been measured with this source, using filters with different transmission curves in the range of interest 1–10 keV. As an example, Fig. 6 shows a spectrum in the range 2–4 keV (red curve) obtained using an Al filter 0.5 μm thick. In the top-right corner, the X-ray transmission as function of the energy is plotted for this filter showing that the absorption goes from 20% to 5% in the range 2.4–4 keV, as measured. The same for Fig. 7, with a thicker Al filter (25 μm) in the range 4–6 keV.

All these spectra can be therefore simulated and an energy calibration curve, relating energy with the peak amplitude, derived.

Spectra have been measured for each pixel when the source operated at HV = 10 kV and placed at
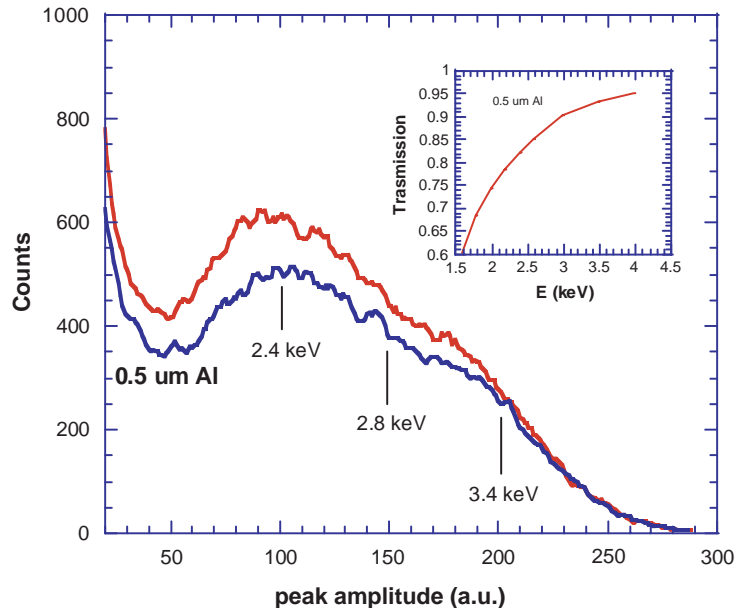
Fig. 6. Pure continuum spectra in the range 2–4 keV, with (blue curve) or without (red curve) a filter of 0.5 μm of Al. Transparency of this filter is shown in the top-right part of the figure.
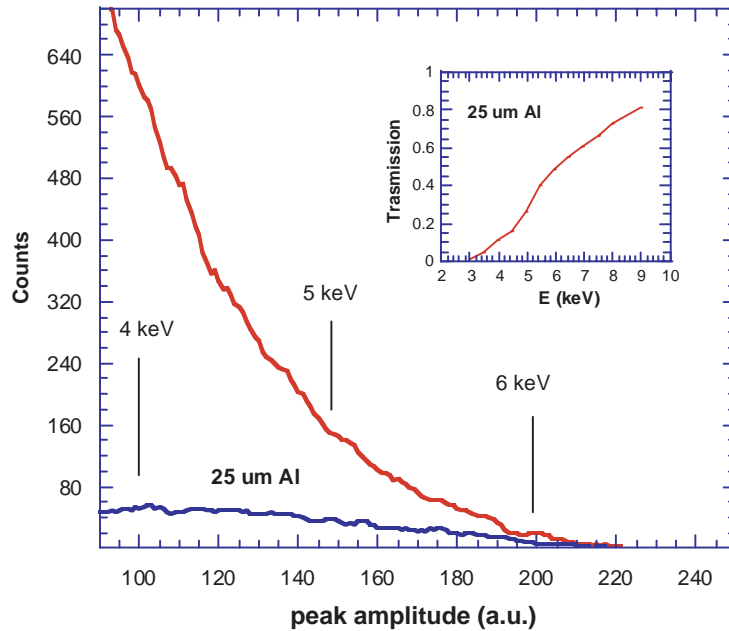
Fig. 7. Pure continuum spectra in the range 4–6 keV, with (blue curve) or without (red curve) a filter of 25 µm of Al. Transparency of this filter is shown in the top-right part of the figure.

10 cm from the detector. The air (10 cm) between the source and the detector affects the continuum spectrum, producing an apparent peak at 3.5 keV (Fig. 8). The gain of the electronic amplifier of each pixel has been adjusted in order to reproduce the same spectrum, with a precision of about 2%, as shown in Fig. 8 just for a few of these pixels. Since each of the 128 channels behaves as an independent spectrometer, this fine electronic calibration is necessary to exploit the combination of imaging capability and energy discrimination, that is one of the most powerful features of this system. Since the energy resolution of the detector in this range is about 20%, the electronic discrimination of the photon energy can be performed with the same uncertainty.

The energy calibration curves, obtained as previously described, are plotted in Fig. 9, for V_{GEM} from 450 to 500 V (different gains) and the gas mixture of Ne 80%–DME 20%, as used in the NSTX experiments. The range of the peak amplitude goes from 20 mV, the threshold to cut off efficiently the electronic noise, to 600 mV, where saturation begins.
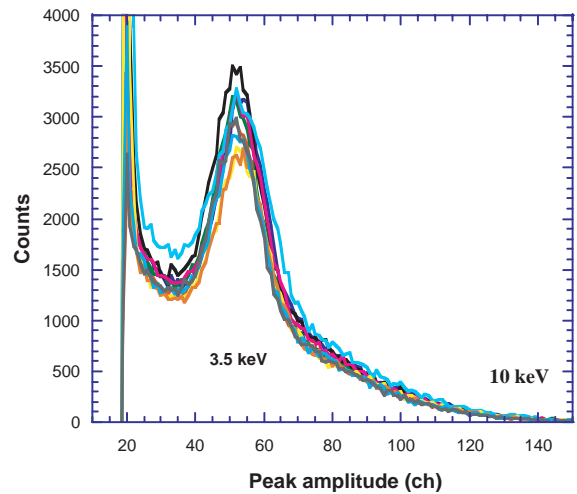
Fig. 8. Adjusting the gain of the amplifiers, all the pixels can produce the same spectrum, as shown in the figure for a few of them, in the range 2–10 keV.

6. Results obtained from NSTX Tokamak plasmas

Results under different plasma conditions will be presented in this paragraph in order to assess the performances of the device.
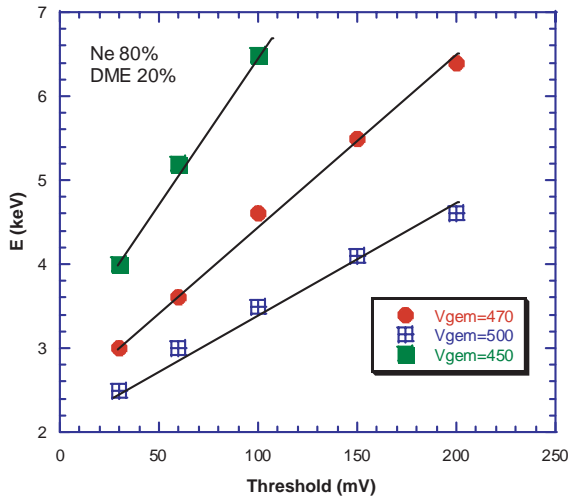
Fig. 9. Energy calibration curves as function of peak amplitude, for three different voltages applied to the gem foil, with a gas mixture of Ne 80% and DME 20%.

NSTX is a spherical Tokamak with major radius 85 cm, minus radius 70 cm and a plasma volume of about 15 m^3. The cross section of the computed nested closed magnetic surfaces is shown in Fig. 10 together with the image of the core obtained with the present device. The plasma has been viewed with different magnifications, from 80 cm × 80 cm (broad view) to 40 cm × 40 cm (zoom) and with different orientations of the optical axis (up, down, in, out). For the case of Fig. 10, the spatial distribution of the photon counts, represented by different colors, is in good agreement with the plasma magnetic reconstructions. It is important to outline this feature because it happens despite the fact that the tangential view in a spherical Tokamak integrates over a large part of the plasma. This very clear 2D picture of the cross section of the plasma core stems from the energy discrimination capability of this device. The effect of image smear out due to the integration of the plasma X-ray emissivity along the line of sight, is indeed strongly reduced by the energy discrimination. In fact, the instrument counts only photons in the range 3–8 keV; since the central electron temperature is not higher than 1.2 keV, the accepted photons come just from the central region, while all the others emitted outside the core, are neglected.
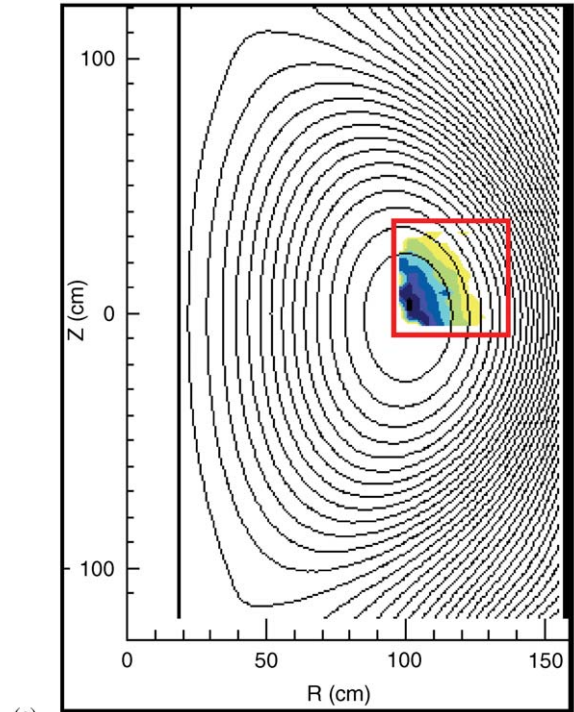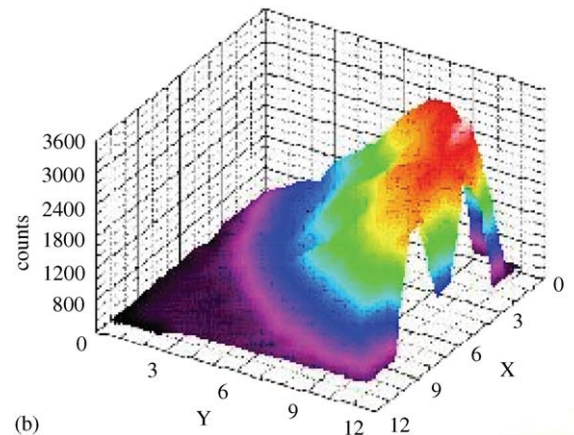
Fig. 10. (a) Color contour plot of the image of a portion of central NSTX plasma (#108727), as obtained with the MPGD system, whose view (red frame) is about 40 cm × 40 cm. The closed magnetic surfaces (solid lines), computed by a magneto-hydrodynamic simulation code, have been superimposed on the X-ray image. (b) 3D plot for a similar case.

Time histories of a few central pixels of the camera are presented in Fig. 11a, with a framing rate of 1 kHz, for a shot with plasma current of
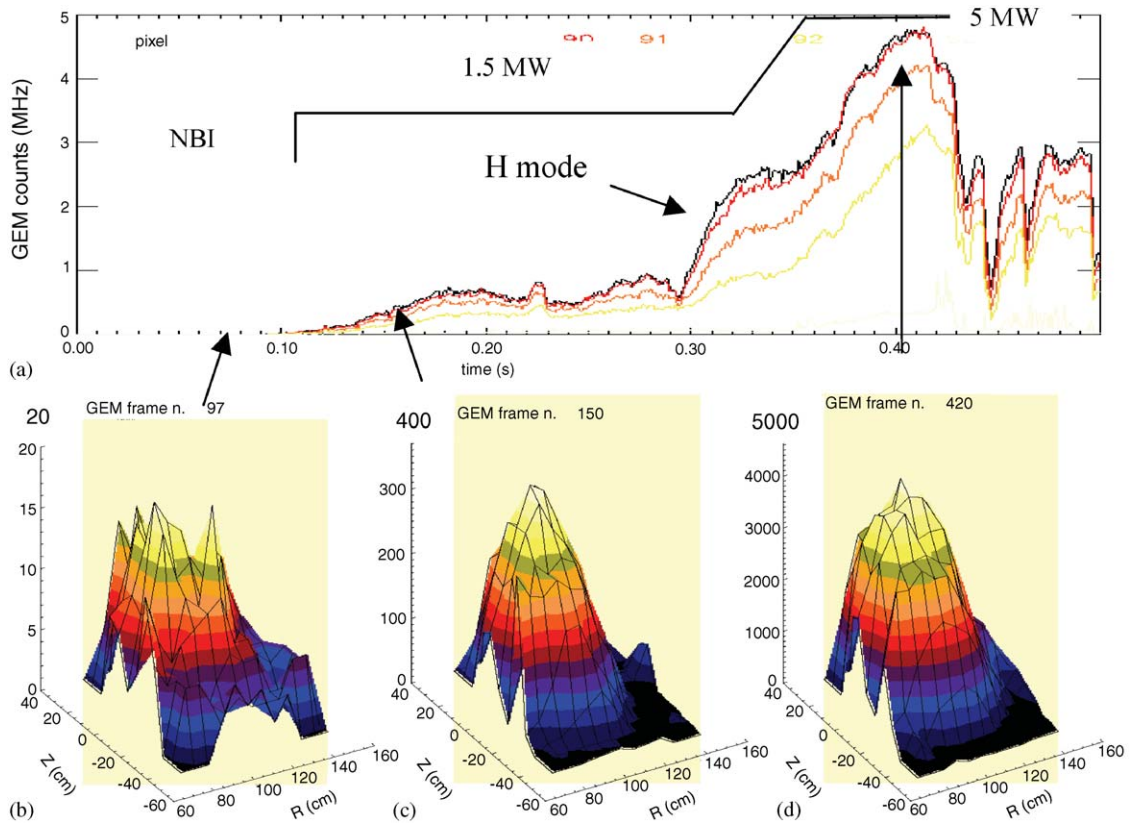
Fig. 11. (a) Time history for a few central pixels during the plasma shot #107314, with the neutral beam injected (NBI) power. 3D plots, at fixed times indicated by the arrows, defining the frame with minimum counts to recognize the plasma (a), an intermediate one (b) and the one with the maximum counts (c) beyond that saturation occurs.

1 MA. The 3D plots of the X-ray emissivities, for a broad view of the core, are shown in Fig. 11a–c at different times: (b) represents the minimum counts to recognize the structure of the core, while (c) the maximum counts (5 MHz/pixel) beyond which saturation occurs (signal pile-up and loss of counting). The spurious counts/pixel of the detector are no more than 5. We can therefore estimate that the signal-to-noise ratio, at the highest emissivity, is about 1000 and the dynamic range of the system is about 250 (from Fig. 11b–d). The capability to get very clear images of the core can be observed also during MagnetoHydroDinamic instability. In Fig. 12a, the time history of a few central pixels, sampled at 1 kHz, is shown, in presence of sawtooth oscillations. The central part of the plasma, measured by means of this instrument, exhibits strong oscillations, while the central lines of sight of a vertical and horizontal perpendicular tomographic array of X-ray diodes show just weak modulations. This enhanced contrast of the image of the central plasma is due to the energy discrimination. In Fig. 12c, the very peaked emissivity profile is shown, just before the onset of the instability.

Increasing the framing rate, the counts per pixel are reduced and the statistical noise increases. A reasonable limit of the framing rate is 100 kHz, where the statistics is still good enough to recognize the structure of the plasma and its dynamics.

7. Conclusion

A new 2D imaging system in the X-VUV range has been set up to diagnose magnetic nuclear fusion plasmas. It is based on a MPGD with a
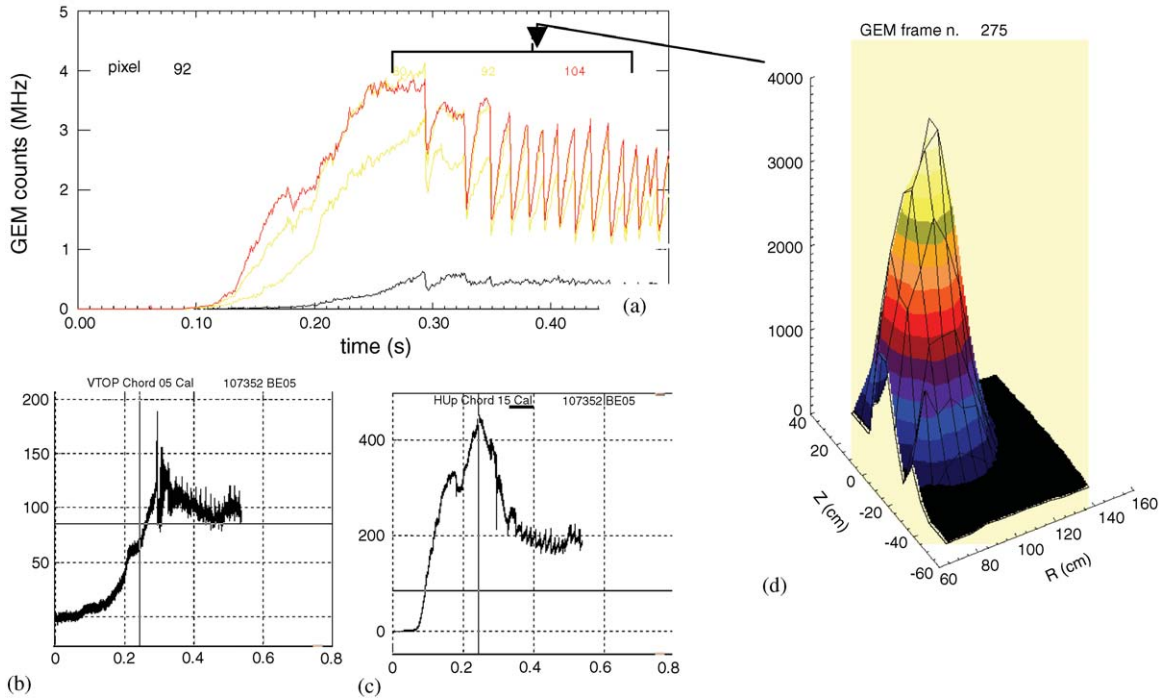
Fig. 12. NSTX shot #107352. (a) Time history, with sampling at 1 kHz, of two central pixels and one peripheral, showing strong central "sawtooth" oscillations. (d) 3D plot of a frame at the time indicated by the arrow, before the onset of the instability. (b,c) central lines of sight of the soft-X-ray tomographic diode arrays, vertical (b) and horizontal (c).

GEM as electron amplifier and a 2D pixel read-out. The energy resolution of the device, which has been tested successfully on FTU and NSTX Tokamaks, has been studied in detail with many X-VUV sources, in the range 0.2–10 keV. The instrument can produce energy discriminated images with very high detected photon flux (10^6 ph/s mm^2). It allows, therefore, high time resolution (framing rate up to 100 kHz) adequate to study fast time scale plasma instabilities. The data obtained on the NSTX experiment confirmed the high dynamic range and signal-to-noise ratio (statistic) and revealed the powerful synergy between imaging capability and energy discrimination. Thanks to these very attractive features and to its flexibility, it can play a role beyond the magnetic plasma physics field.

Acknowledgements

References

[1] D. Pacella, et al., Rev. Sci. Instrum. 72 (2) (2001).
[2] R. Bellazzini, et al., Nucl. Instr. and Meth. A 471 (2001) 41.
[3] F. Sauli, Nucl. Instr. and Meth. A 419 (1998) 189.
[4] V. Pericoli-Ridolfini, et al., Phys. Rev. Lett. 82 (1999) 93.
[5] P. Buratti, et al., Phys. Rev. Lett. 82 (1999) 560.
[6] S.A. Sabbagh, et al., Nucl. Fusion 41 (2001) 1197.
[7] M. Ono, et al., Nucl. Fusion 40 (2000) 557.